

# Effects of square micro-pillar array porosity on the liquid motion of near surface layer\*

Xiaoxi Qiao(乔小溪)<sup>1,†</sup>, Xiangjun Zhang(张向军)<sup>2</sup>, Ping Chen(陈平)<sup>1</sup>, Yu Tian(田煜)<sup>2</sup>, and Yonggang Meng(孟永钢)<sup>2</sup>

<sup>1</sup>School of Mechanical Engineering, University of Science and Technology Beijing, Beijing 100083, China

<sup>2</sup>State Key Laboratory of Tribology, Tsinghua University, Beijing 100084, China

(Received 18 September 2019; revised manuscript received 23 October 2019; accepted manuscript online 9 December 2019)

The influence rules of square micro-pillar array porosity on the liquid motion characteristics of the near-surface layer are investigated by quartz crystal microbalance (QCM). QCM is a powerful and promising technique in studying the interfacial behavior, which exhibits great advantages in investigating the effects of surface microstructure, roughness, and array. In our experiments, three different arrays with the same height of about 280 nm and center distance of 200  $\mu\text{m}$ , but different diameters of about 78  $\mu\text{m}$ , 139  $\mu\text{m}$ , and 179  $\mu\text{m}$  are investigated. The results indicate that when the surface array has a large porosity, its influence on the liquid motion of the near surface layer is slight, thus resulting in a small increase of half-bandwidth variation due to the additional friction energy dissipation. When the surface array has a small porosity, the array tends to make the liquid film trapped in the array oscillating with the substrate, then there may be a layer of liquid film behaving like rigid film, and it also will make the liquid motion near the array layer more complicated. Thus for the #3 surface with a small porosity, both the absolute values of frequency shift  $|\Delta f_3|$  and half-bandwidth variation  $\Delta \Gamma_3$  increase obviously. The experimental results show good consistence with the theoretical model of Daikhin and Urbakh. This study sheds light on understanding the influence mechanism of surface array porosity on the liquid motion of near-surface layer.

**Keywords:** quartz crystal microbalance, square micro-pillar array, wetting state, permeability

**PACS:** 47.55.dr, 47.54.De

**DOI:** 10.1088/1674-1056/ab5fba

## 1. Introduction

Study on liquid flowing behaviors through micro/nano-scale arrays has received significant interest due to its broad application in the fields of microfluidic, tribology, liquids mixing, flow drag reduction, and so on. So far, many methods have been developed to fabricate micro/nano-scale array patterned surfaces, such as photolithography, focused ion beam (FIB) lithography, e-beam lithography, plasma-etching, and laser machining technique. The micro/nano-scale array can also significantly affect the liquid interfacial behaviors, like adhesion, surface wetting, shear viscous resistance, interfacial slip, etc. Researches indicate that the rib structure patterned in the micro-channel can significantly influence the liquid flow characteristics and reduce the friction drag of liquid flowing through the surface.<sup>[1,2]</sup> And the lotus-leaf-like dual-scale structure fabricated on the solid surface can alter the surface wetting property and realize the super-hydrophobicity, anti-icing, waterproofing, self-cleaning, and low adhesion.<sup>[3–6]</sup> Lee *et al.* improved the storage properties of lithium-ion battery by modifying the battery electrodes with stripe- and square-patterned arrays of SnO<sub>2</sub> nanowires for its ability of promoting the diffusion of the liquid electrolyte.<sup>[7]</sup> The surface with micro/nanoscale array can regulate the adsorption of protein, the adhesion, migration, and spreading behaviors of the cell, and so on.<sup>[8]</sup> Meanwhile, a patterned surface can greatly affect

the performance of lubrication, friction, and carrying capacity of the motion pair.<sup>[9–11]</sup>

For regular microstructure arrays, it can be classed into two types of micro-pillar (discrete) and micro-dimple (continuous) according to the distribution modes of solid part. In the paper, we mainly focus on the square micro-pillar arrays. The micro-pillar array has received extensive attention in both the academia and industry, especially in the microfluidic system. When the solid surface is patterned with micro/nano-pillar arrays, it will inevitably influence the interfacial behaviors of the liquid in contact with the solid surface. Thus comprehensive understanding the influence mechanism of the micro/nano-scale array on the liquid–solid interaction and liquid flowing characteristics is of great importance. So far, there are many experimental and theoretical research methods for studying the micro/nano-pillar arrays. In our paper, the experimental instrument used is quartz crystal microbalance (QCM). QCM is a powerful technique in investigating the solid–liquid interfacial behaviors. Meanwhile, the establishment of the theoretical model for rough surface<sup>[12,13]</sup> makes QCM a promising technology in studying the effect of the microstructure arrays. Here, we investigate the influence rules of the square micro-pillar array porosity on the liquid flowing behaviors of a near-surface layer based on the QCM technique.

\*Project supported by the National Natural Science Foundation of China (Grant No. 51905032), the National Key Research and Development Program of China (Grant No. 2018YFC0810500), and the Fundamental Research Funds for the Central Universities, China (Grant No. FRF-TP-18-012A2).

†Corresponding author. E-mail: [qx41051134@126.com](mailto:qx41051134@126.com)

## 2. Experimental section

### 2.1. Instrument

Experiments are conducted by QCM (Z-500, KSV, Finland). And the schematic diagram of QCM is shown in Fig. 1. For all experiments, the QCM chips are cleaned by Acetone, alcohol, and deionized water in turn, then dried with high pure  $N_2$ .

QCM is a powerful and promising technique in investigating the interfacial behaviors of the near-surface liquid layer with high accuracy and sensitivity.<sup>[14]</sup> Any tiny change occurring on the chip surface will result in frequency shift  $\Delta f_N$  and half-bandwidth variation  $\Delta\Gamma_N$  of the QCM system. Thus the  $\Delta f_N$  and  $\Delta\Gamma_N$  can be used to reveal the physical properties of the interfacial layer, and the influence rule of the surface array density on the liquid flowing behaviors of the near surface layer. The relationships among  $\Delta f_N$ ,  $\Delta\Gamma_N$ , and surface mechanical impedance  $Z_s$  are

$$\Delta f_N = \frac{-f_0}{\pi(\mu_q \rho_q)^{1/2}} \text{Im}(Z_s), \quad (1)$$

$$\Delta\Gamma_N = \frac{f_0}{\pi(\mu_q \rho_q)^{1/2}} \text{Re}(Z_s), \quad (2)$$

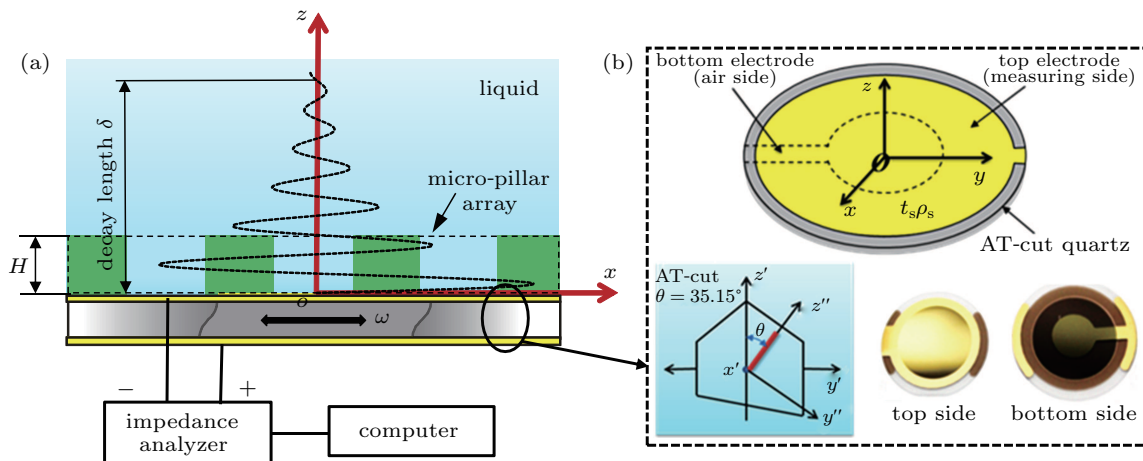


Fig. 1. Diagram of (a) the QCM device and (b) the QCM chip.

Table 1. Density and viscosity of the water-sucrose solutions used in the experiments (20 °C).

Mass concentration	Density $\rho/\text{g}\cdot\text{cm}^{-3}$	Viscosity $\eta/\text{mPa}\cdot\text{s}$	$\rho\eta/(\text{kg}^2/(\text{m}^4\cdot\text{s}))$	Decay length/nm
0	1.00	1.03	1.03	147.9
9.6%	1.038	1.34	1.39	165.6
18.3%	1.074	1.85	1.99	191.2
27%	1.115	2.72	3.03	227.6

### 2.3. Fabrication and characterization of the square micro-pillar array surface

In this paper, the cylindrical micro-pillar arrays in square-packed arrangements are adopted, as shown in Fig. 2(a), and the micro-pillar arrays are along or perpendicular to the vibration direction of the quartz crystal as the arrow indicates.  $L$  is the center distance between two adjacent cylinders,  $D$  is

where  $\mu_q$  and  $\rho_q$  are the shear elastic modulus and density of the quartz crystal, respectively, and  $f_0 = 5$  MHz is the fundamental resonant frequency.  $N$  is the resonator harmonic number ( $N = 1, 3, 5, 7, 9, 11$ ). Surface mechanical impedance  $Z_s$  is related with the properties of the tested surface load, given by  $Z_s = \frac{T_{xy}}{v_q}|_{z=0}$ . The real part of  $Z_s$  represents energy dissipation relating with the half-bandwidth  $\Gamma$ , and its imaginary part characterizes the storage energy and inertial mass relating with the resonant frequency. Thus, for a rigid film distributing uniformly on the chip surface with its thickness much less than that of the QCM chip,  $\Delta\Gamma = 0$ , and  $\Delta f_N = \frac{-2Nf_0^2}{(\mu_q \rho_q)^{1/2}} \rho_s$  ( $\rho_s$  is the film mass density). For a pure viscous liquid load on a smooth chip surface,  $\Delta f_N = -\Delta\Gamma_N = -N^{1/2} f_0^{3/2} (\frac{\rho\eta}{\pi\rho_q \mu_q})^{1/2}$ .

### 2.2. Preparation and characterization of liquid samples

In our experiments, the mass concentrations of water-sucrose solutions used are 0, 9.6%, 18.3%, and 27%, and the solutions are prepared with chemically pure sucrose and deionized water. Their densities and viscosities are measured by a density meter and Rheometer (MCR 301, Anton Paar GmbH, Germany) respectively, as shown in Table 1.

the diameter of the micro-cylinder, and  $H$  is the height of the arrays. The patterned surfaces are measured by a white light interferometer with their 3D surface topographies and detailed sizes shown in Fig. 2 and Table 2, respectively. The surface arrays are fabricated by photolithography. The materials of the micro-pillar arrays and the substrate surface are Cr and Au, respectively.

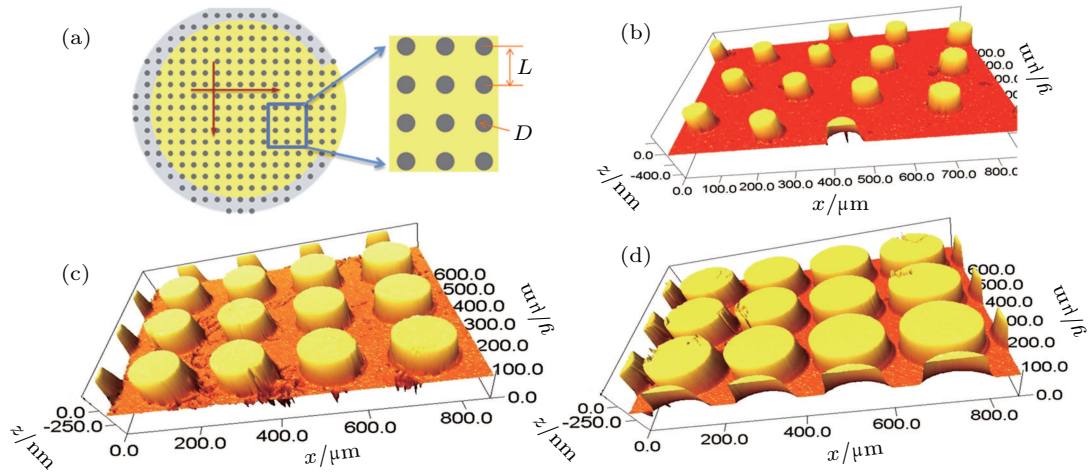


**Fig. 2.** (a) Schematic illustration of the square array distributed on QCM chip surface, and the 3D surface images with (b)  $D = 78 \mu\text{m}$ , (c)  $D = 139 \mu\text{m}$ , (d)  $D = 179 \mu\text{m}$  measured by white light interference.

Further, the surface arrays can be treated as a porous film, and characterized by permeability. Permeability describes the viscous resistance of liquid flowing through the surface arrays, which depends on the porosity, pillar shape, arrangement, and size of the arrays, and has nothing to do with the liquid properties. In this paper, the equation used to calculate the permeability of the square micro-cylinder array is<sup>[15]</sup>

$$\frac{K}{D^2} = \frac{0.0602\pi\phi^{5.1}}{4(1-\phi)}, \quad (3)$$

where  $K = \xi_H^2$  is the permeability, and  $\phi$  is the porosity. For a square micro-cylinder array, the porosity is  $\phi = 1 - \pi D^2/4L^2$ . Then the corresponding  $\xi_H^2$  for the surface arrays we used is given in Table 2.

**Table 2.** The size, porosity, and permeability of the square micro-pillar arrays used in experiments.

No.	Array	$H/\text{nm}$	Porosity	$\xi_H^2/\mu\text{m}^2$
#1	$D = 78 \mu\text{m}, L = 200 \mu\text{m}$	280	0.88	1258.8
#2	$D = 139 \mu\text{m}, L = 200 \mu\text{m}$	280	0.62	211.7
#3	$D = 179 \mu\text{m}, L = 200 \mu\text{m}$	280	0.37	15.4

### 3. Results and discussion

#### 3.1. Characterization of the surface wetting state

Firstly, the wetting properties of the patterned surfaces are characterized as shown in Fig. 3. The contact angles of  $3 \mu\text{L}$  deionized water on the patterned surfaces are in the range of  $60^\circ$ – $65^\circ$ . And, all the three surfaces are in Wenzel wetting state, which can be obtained by observing the receding triple line in the evaporating process of the water droplet. As Fig. 3 shows, the #3 surface receding triple line shows obvious pinning effect around the cylindrical pillar, meanwhile there are water ripples in the gap between the adjacent pillars. Both the above phenomena indicate that the #3 surface is in Wenzel wetting state, which means that the liquid can fill into the gap. As the #3 surface has the highest density, thus we can deduce that both the #1 and #2 surfaces are in Wenzel wetting state.

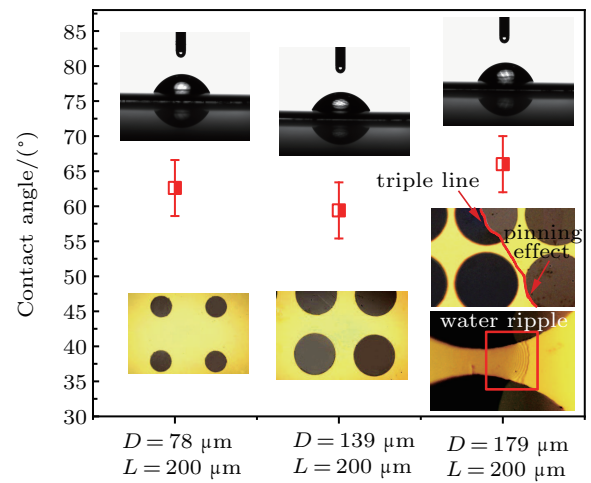


**Fig. 3.** Contact angles and wetting state of the patterned surfaces used in experiments.

#### 3.2. QCM experiments

Figure 4 shows the experimental  $\Delta f_N$  and  $\Delta\Gamma_N$  of  $N = 3$  varying with the product of density  $\rho_1$  and viscosity  $\eta_1$  of the water-sucrose solutions for the three array surfaces. Here, the  $\Delta f_3$  and  $\Delta\Gamma_3$  respectively are the relative changes of the system resonant frequency and half-bandwidth from without liquid load to with liquid load. Figure 4 indicates that the higher  $\rho_1\eta_1$  results in the larger absolute value of frequency shift  $|\Delta f_3|$  and half-bandwidth variation  $\Delta\Gamma_3$ . And for the same  $\rho_1\eta_1$ , the  $\Delta\Gamma_3$  increases with the diameter of the micro-cylinder increasing. But the  $|\Delta f_3|$  firstly decreases slightly and then increases with the diameter of the micro-cylinder increasing. For the surfaces with  $D = 78 \mu\text{m}$  and  $D = 139 \mu\text{m}$ , the absolute frequency shifts are slightly smaller than that of the smooth surface. For the surface with  $D = 179 \mu\text{m}$ , its  $|\Delta f_3|$  is much larger than that of the smooth surface. And the increment of  $\Delta\Gamma_3$  caused by increasing array density is obviously larger than the increment of  $|\Delta f_3|$ .

The  $\Delta f$  and  $\Delta\Gamma$  are close related with the flow characteristics of the near-surface liquid layer. Both inertial and viscous

components contribute to the QCM responses. When the chip surface is patterned with micro-pillar arrays, it will inevitably influence the liquid motion of near surface layer and makes it more complicated, such as the generation of non-laminar motion, trapping of liquid in the gap between micro-pillars, and the conversion of the in-plane surface motion into the surface-normal liquid motion. The liquid flowing behaviors depend on the array porosity, shape, height, arrangement, and so on. Here, we mainly focus on the effect of the array porosity (or density) on the liquid motion.

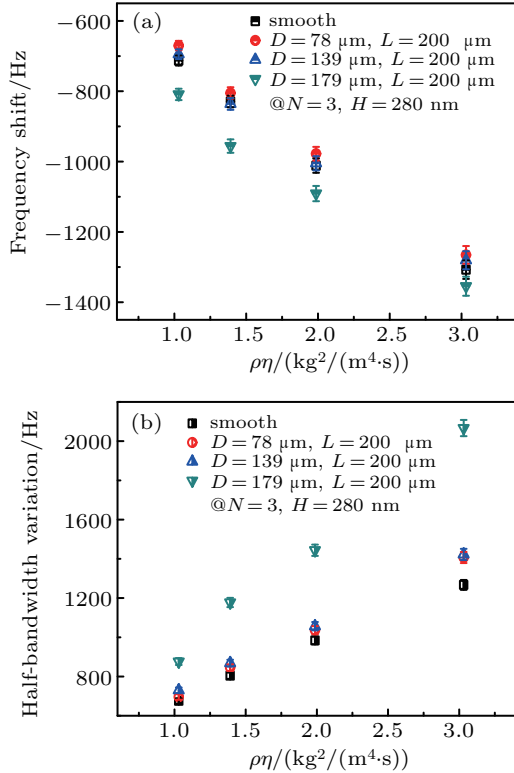


**Fig. 4.** (a) Experimental frequency shift and (b) half-bandwidth variation varying with the product of density and viscosity at  $N = 3$ .

For the #1 and #2 surfaces with large porosity, the effects of the array on liquid motion are relatively small. Even so, the arrays still have a tiny influence on the liquid motion and make it more chaos, and the patterned array increases the solid-liquid contact area, resulting in larger friction energy loss, thus their half-bandwidth variations  $\Delta f_3$  show a slight increment, but the frequency shifts  $|\Delta f_3|$  are almost the same as those for the smooth surface, and even show a tiny decrease. This is because the half-bandwidth is related with system energy dissipation, and the frequency shift is related with system energy storage.

For the #3 surface with a small porosity, both the frequency shift  $|\Delta f_3|$  and  $\Delta f_3$  show an obvious increase. In this condition, the array tends to confine the liquid in the gap of the micro-pillar and makes the near surface liquid layer oscillating synchronously with the substrate. Then it will result in more energy storage in the kinetic form, thus resulting in large

frequency shift  $|\Delta f_3|$ . Meanwhile, the trapped liquid film can be recognized as a rigid film coupled with the substrate, as shown in Fig. 5. And then the system frequency shift includes two parts as follows:

$$\Delta f = \Delta f_{\text{tr}} + \Delta f_1 = -\frac{2Nf_0^2}{(\mu_q \rho_q)^{1/2}} \rho_s - N^{1/2} f_0^{3/2} \left( \frac{\rho \eta}{\pi \rho_q \mu_q} \right)^{1/2}. \quad (4)$$

The first term  $\Delta f_{\text{tr}}$  is the frequency shift caused by the trapped liquid film coupled rigidly to the substrate. The second term  $\Delta f_1$  is the frequency shift caused by the ‘free’ oscillating liquid layer, the same as that for the smooth surface.  $\rho_s$  is the mass density, i.e., trapped liquid mass per unit area, which is related with the array porosity  $\phi$ , the density  $\rho_l$  and height  $h$  of the trapped liquid film, i.e.,  $\rho_s = \rho_l h \phi$ . Noticeably, this height  $h$  is always smaller than the array height  $H$ , and usually there is no an obvious boundary between the ‘rigid’ liquid film and the ‘free’ liquid layer, as shown in Fig. 6.

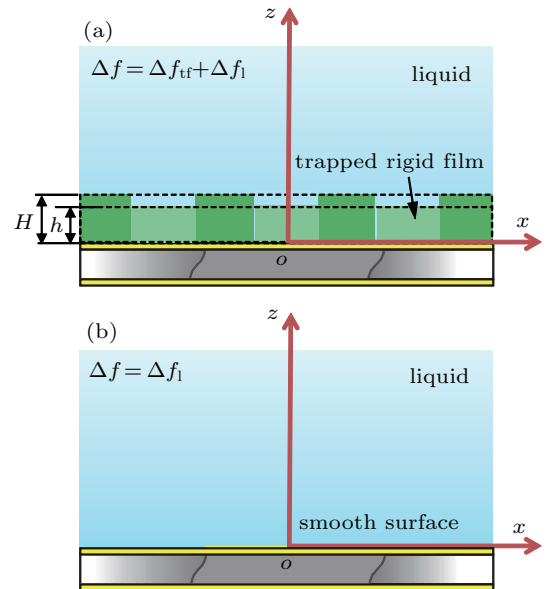


**Fig. 5.** Schematic of frequency shifts for (a) surface with micro-pillar porous film and (b) smooth surface.

Meanwhile, the array with small porosity makes the liquid motion of the solid-liquid interfacial layer more complicated, thus resulting in larger energy dissipation and higher half-bandwidth variation. According to the theory of Daikhin and Urbakh,<sup>[12]</sup> we obtain the liquid velocity  $v_x(z, \omega)$  of the near surface layer along the  $z$  direction, as shown in Fig. 6. In the theory, the array is treated as a porous film, and the influences of the array porosity, shape, and arrangement are effectively included into the permeability. In this paper, we focus on the effects of the array porosity (or density), and higher porosity corresponds to larger permeability, as Table 2 shows.

The relative velocity in Fig. 6 is the ratio of liquid velocity  $v_x(z, \omega)$  to liquid velocity  $V_0$  at the interface  $Z = 0$ . From Fig. 6 we can see that when the permeability is large enough,

the effect of the arrays on the liquid motion can be neglected. With the permeability decreasing, the array will make the liquid motion more chaos, and tend to make the near surface liquid layer oscillating with the substrate, which means the confinement effect of the micro-pillar arrays on the liquid motion becomes strong. When the permeability is small enough, there is a liquid layer rigidly coupled to the substrate surface.

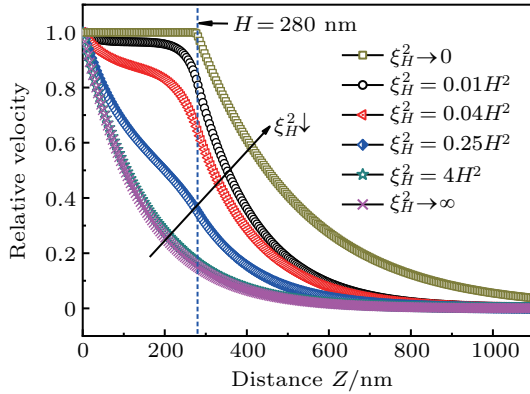


Fig. 6. Effects of array permeability on the liquid velocity profile along the vertical distance  $Z$ .

It is also worth noting that the liquid motion along the chip surface plane is treated approximately as macroscopically homogeneous in the theory. But in fact, the liquid in the array layer shows complicated flowing behaviors around the micro-pillar and also disturbs the liquid motion near the array layer. Thus it will present more energy dissipation caused by the disturbed non-laminar flowing and the friction between liquid and solid phase in the layer. The half-bandwidth variation depends on the energy dissipation, therefore, the #3 surface shows a high half-bandwidth variation.

Further, we introduce a dimensionless permeability  $\xi_H'^2 = \xi_H^2 / \delta^2$  ( $\delta = \sqrt{2\eta_1 / \rho_1 \omega}$  is the decay length,  $\eta_1$  and  $\rho_1$  are the viscosity and density of the tested liquid, respectively, and  $\omega$  is the angular frequency) to normalize the experimental results. The normalized frequency shift and normalized half-bandwidth variation are defined as the ratios of  $\Delta f_N$  and  $\Delta \Gamma_N$  for the array surface to those for the smooth surface, respectively. Finally, the influence rule of  $\xi_H'^2$  on the normalized frequency shifts and normalized half-bandwidth variations are obtained, as shown in Fig. 7.

From Fig. 7, we can see that both the normalized frequency shift and normalized half-bandwidth variation increase with the dimensionless permeability  $\xi_H'^2$  decreasing, the same change trend with the theoretical results given in Ref. [12]. This study sheds light on the influence mechanism of micro-pillar density on the near surface liquid layer, which helps us to better understand and control the liquid flowing and mixing by using a micro-structure.

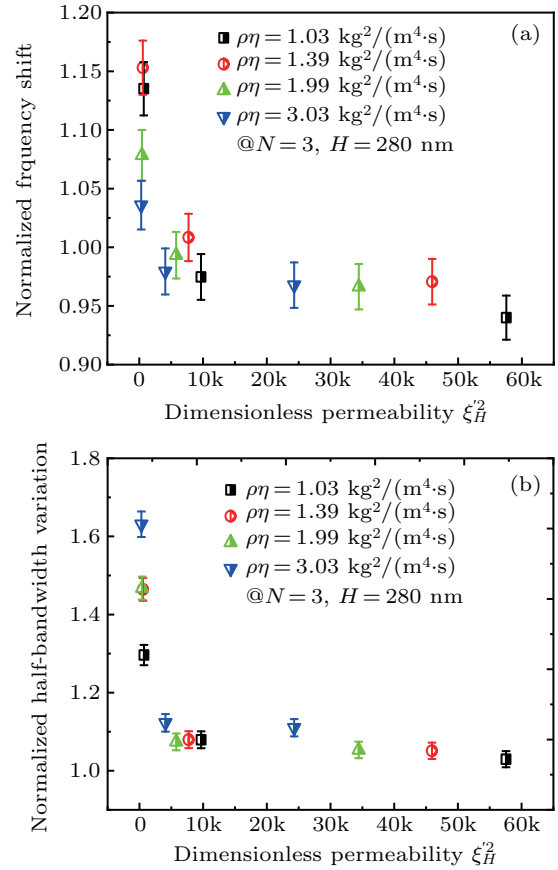


Fig. 7. Normalized frequency shift and normalized half-bandwidth variation varying with the dimensionless permeability  $\xi_H'^2$ .

#### 4. Conclusion and perspectives

QCM, as a powerful technique in investigating solid-liquid interfacial properties, can be used to study the liquid flowing behaviors through the array layer according to the system frequency shift and half-bandwidth variation. In this paper, we fabricate three square micro-pillar arrays with different diameters, same height of about 280 nm, and same center distance of 200  $\mu\text{m}$ . Firstly, the wetting properties of the array surfaces are investigated. The results indicate that the three array surfaces have the similar contact angle in the range of  $60^\circ - 65^\circ$ . And all their wetting states are in the Wenzel regime, i.e., liquid can fall into the gap between the micro-pillars and flow through them.

Next, we study experimentally the influences of the micro-pillar array porosity on the liquid motion. According to the literatures, when the array height  $H$  we used in experiments is larger than the decay length for all the liquid samples, the chip surface cannot be treated as hydrodynamic smooth. However, in this paper, the array we used is obvious larger than the array height. Meanwhile, the effects of the array on the liquid flowing behavior are related with the array porosity, shape, and arrangement. Here we mainly focus on the effects of porosity. In our experiment, for the #1 and #2 surfaces with large porosity, they have tiny effects on the liquid motion,

which results in a small incensement of the half-bandwidth variation due to additional energy dissipation. For the #3 surface with a small porosity, it has a significantly influence on the liquid motion of the near surface layer, tends to confine the liquid motion in the array layer, and makes a certain thickness of liquid film rigidly coupled to the substrate. Meanwhile, the liquid in the array layer shows complicated flowing behaviors and disturbs the liquid motion near the array layer, thus both the absolute values of frequency shift and half-bandwidth variation show obvious increase. The experimental results show the same tendency with the theory of Daikhin and Urbakh, which treats the array as a porous film and adopts permeability to describe effectively the influence of the array porosity, shape, and arrangement.

## References

- [1] Priezjev N V 2011 *J. Chemical Physics* **135** 204704
- [2] Yamada T, Hong C, Gregory O J and Faghri M 2011 *Microfluid. Nanofluid.* **11** 45
- [3] Jung Y C and Bhushan B 2010 *J. Phys. Condens. Matter An Inst. Phys. J.* **22** 35104
- [4] Lyu S, Dang C N, Kim D, Hwang W and Yoon B 2013 *Appl. Surf. Sci.* **286** 206
- [5] Ou J, Perot B and Rothstein J P 2004 *Phys. Fluids* **16** 4635
- [6] Woolford B, Prince J, Maynes D and Webb B W 2009 *Phys. Fluids* **21** 85106
- [7] Lee S H and Kim W B 2016 *J. Power Sources* **307** 38
- [8] Anselme K 2000 *Biomaterials* **21** 667
- [9] Suh M S, Chae Y H, Kim S S, Hinoki T and Kohyama A 2010 *Tribol. Int.* **43** 1508
- [10] Wakuda M, Yamauchi Y, Kanzaki S and Yasuda Y 2003 *Wear* **254** 356
- [11] Zhao Y P 2012 *Physical Mechanics of Surfaces and Interfaces* (Beijing: Science Press) (in Chinese)
- [12] Daikhin L and Urbakh M 1996 *Langmuir* **12** 6354
- [13] Daikhin L, Gileadi E, Katz G, Tsionsky V, Urbakh M and Zagidulin D 2002 *Anal. Chem.* **74** 554
- [14] Qiao X X, Zhang X J, Tian Y and Meng Y G 2016 *Appl. Physics Reviews* **3** 031106
- [15] Sahaoui M, Kaviany M, Mechanics A and Arbor A 1992 *Int. J. Heat Mass Britain* **35** 927